nature neuroscience

TACE (ADAM17) inhibits Schwann cell myelination

Rosa La Marca[1,2], Federica Cerri[1,2], Keisuke Horiuchi[3], Angela Bachi[4], M Laura Feltri[4], Lawrence Wrabetz[4], Carl P Blobel[5], Angelo Quattrini[1,2], James L Salzer[6–8] & Carla Taveggia[1,2]

Tumor necrosis factor-α–converting enzyme (TACE; also known as ADAM17) is a proteolytic sheddase that is responsible for the cleavage of several membrane-bound molecules. We report that TACE cleaves neuregulin-1 (NRG1) type III in the epidermal growth factor domain, probably inactivating it (as assessed by deficient activation of the phosphatidylinositol-3-OH kinase pathway), and thereby negatively regulating peripheral nervous system (PNS) myelination. Lentivirus-mediated knockdown of TACE *in vitro* in dorsal root ganglia neurons accelerates the onset of myelination and results in hypermyelination. In agreement, motor neurons of conditional knockout mice lacking TACE specifically in these cells are significantly hypermyelinated, and small-caliber fibers are aberrantly myelinated. Further, reduced TACE activity rescues hypomyelination in NRG1 type III haploinsufficient mice *in vivo*. We also show that the inhibitory effect of TACE is neuron-autonomous, as Schwann cells lacking TACE elaborate myelin of normal thickness. Thus, TACE is a modulator of NRG1 type III activity and is a negative regulator of myelination in the PNS.

Myelin, the insulating membrane that is produced by Schwann cells in the PNS and by oligodendrocytes in the CNS, is an organelle whose assembly and function is crucial for proper transmission of the electric impulse. Myelination in the PNS is controlled at the molecular level by the amount of axonal NRG1 type III[1,2]. Thus, clarifying the mechanisms that control NRG1 type III expression is essential to establish the molecular events that regulate myelin formation. The β-secretase BACE1 (refs. 3–5) and the α-secretases belonging to the ADAM family of proteases[6] control the classical regulated proteolysis of NRG1. Although the role of BACE1 in NRG1 type III cleavage has been investigated during myelination and remyelination[3–5], the role of the α-secretases is unclear.

ADAM (a disintegrin and metalloprotease) proteins are a family of zinc-dependent, membrane-anchored metalloproteases that are implicated in ectodomain shedding of several growth factors. ADAMs control myogenesis, neurogenesis, fertilization, inflammation and myelination[6]. Several members of the ADAM secretases are expressed in the PNS, and some have been implicated in myelination. In particular, ADAM19 can process NRG1 (ref. 7), although recent studies suggest that ADAM19 targets NRG1 type I[8], which is not implicated in myelination[1,2]. Accordingly, mice lacking ADAM19 myelinate normally, although they have delayed remyelination[9]. Another ADAM that is directly implicated in myelination is ADAM22, as transgenic mice lacking ADAM22 are hypomyelinated in the PNS[10]. However, it is unlikely that ADAM22 cleaves NRG1 type III or other growth factors, as this protein lacks a catalytic-site consensus sequence[6]. Rather, axonal ADAM22 functions as a receptor for secreted LGI4 (leucine-rich repeat LGI family, member 4)[11]. Recently, the role of ADAM10 in NRG1 cleavage was analyzed. However, mice with altered ADAM10 expression myelinate normally in the PNS[12], suggesting that ADAM10 is dispensable for this process.

Another member of this family, TACE, has been implicated in NRG1 cleavage[13]. TACE mediates ectodomain shedding of several membrane-bound molecules, including tumor necrosis factor-α (TNF-α), transforming growth factor-α (TGF-α), p75 neurotrophin receptor ($p75^{NTR}$; also known as NGFR), Notch and amyloid precursor protein (APP)[6,14] in addition to NRG1. Transgenic mice lacking TACE die at birth, preventing the analysis of myelination *in vivo*[15]. We now report that TACE cleaves NRG1 type III and that ablation of TACE results in altered processing of axonal NRG1 type III. In addition, downregulation of TACE expression *in vitro* in myelinating cocultures and inactivation of TACE *in vivo* in motor neurons lead to precocious myelination, hypermyelination, ectopic myelination and enhanced activation of the phosphatidylinositol-3-OH kinase (PI3K) pathway. Furthermore, the reduction of TACE activity *in vivo* is sufficient to rescue myelination of NRG1 type III haploinsufficient mice. We also provide evidence that this phenotype is due to a cell-autonomous mechanism, as inactivation of TACE in Schwann cells *in vitro* and *in vivo* does not alter the timing of myelin production or the amount produced.

Thus, our study reveals a previously uncharacterized role for TACE in myelination. By cleaving NRG1 type III, TACE determines the amount of this critical regulator of myelination on the axonal surface and, unlike BACE1 (refs. 3,5), negatively regulates PNS myelination. To our knowledge, this is the first study reporting a negative mechanism for controlling NRG1 type III expression and myelination, further suggesting that secretases are important modulators of myelination.

[1]Division of Neuroscience, San Raffaele Scientific Institute, Milan, Italy. [2]Institute of Experimental Neurology, San Raffaele Scientific Institute, Milan, Italy. [3]Department of Orthopedic Surgery, School of Medicine, Keio University, Tokyo, Japan. [4]Division of Genetics and Cell Biology, San Raffaele Scientific Institute, Milan, Italy. [5]Arthritis and Tissue Degeneration Program, Hospital for Special Surgery at Weill Medical College of Cornell University, New York, New York, USA. [6]Department of Cell Biology, New York University School of Medicine, New York, New York, USA. [7]Department of Neurology, New York University School of Medicine, New York, New York, USA. [8]Smilow Neuroscience Program, New York University School of Medicine, New York, New York, USA. Correspondence should be addressed to C.T. (taveggia.carla@hsr.it).

Received 14 February; accepted 7 April; published online 12 June 2011; doi:10.1038/nn.2849

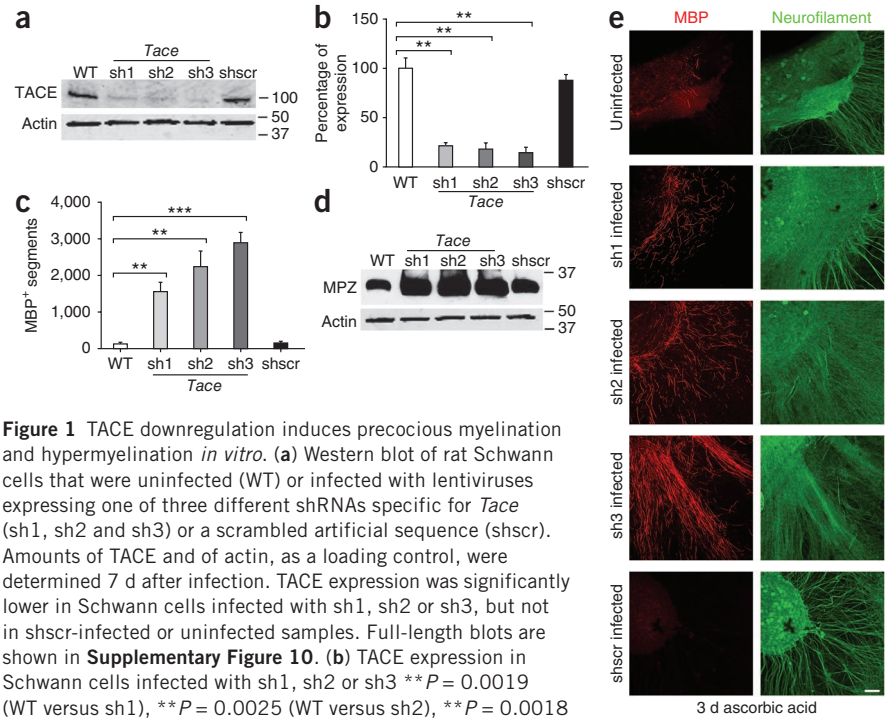

Figure 1 TACE downregulation induces precocious myelination and hypermyelination *in vitro*. (**a**) Western blot of rat Schwann cells that were uninfected (WT) or infected with lentiviruses expressing one of three different shRNAs specific for *Tace* (sh1, sh2 and sh3) or a scrambled artificial sequence (shscr). Amounts of TACE and of actin, as a loading control, were determined 7 d after infection. TACE expression was significantly lower in Schwann cells infected with sh1, sh2 or sh3, but not in shscr-infected or uninfected samples. Full-length blots are shown in **Supplementary Figure 10**. (**b**) TACE expression in Schwann cells infected with sh1, sh2 or sh3 $^{**}P = 0.0019$ (WT versus sh1), $^{**}P = 0.0025$ (WT versus sh2), $^{**}P = 0.0018$ (WT versus sh3). Data shown are the averages of three experiments; error bars, mean ± s.e.m. (**c**) Quantification of MBP-positive segments 3 d after the induction of myelination in control cultures and cultures infected with *Tace* shRNA or shscr. Quantification was performed on the entire culture (a total of three coverslips per experiment) $^{**}P = 0.0012$ (WT versus sh1), $^{**}P = 0.0047$ (WT versus sh2), $^{***}P < 0.0001$ (WT versus sh3). Data shown are averages of three experiments; error bars, mean ± s.e.m. (**d**) Western blot of organotypic rat Schwann cell neuronal cocultures that were uninfected or infected with lentiviruses expressing sh1, sh2 or sh3, or shscr. Lysates were tested for MPZ, and for actin as a loading control, 14 d after the induction of myelination. MPZ expression was significantly upregulated in cultures in which TACE was knocked down. (**e**) Organotypic rat Schwann cell neuronal cocultures infected with lentiviruses expressing *TACE*-specific shRNAs or shscr were maintained in myelinating conditions for 3 d, fixed and stained for MBP (rhodamine) and neurofilament (fluorescein). Numerous myelin segments were evident in *Tace* shRNA–infected cultures; none formed in shscr-infected cultures and only a few formed in uninfected cultures. Scale bar, 100 μm.

RESULTS

TACE inactivation enhances myelination *in vitro*

To investigate the role of TACE in myelination, we first analyzed its mRNA and protein levels *in vitro*. TACE is highly expressed in Schwann cells and, at lower levels, in dorsal root ganglia (DRG) neurons, as shown by PCR with reverse transcription (RT-PCR) and western blot analyses of cDNAs or lysates prepared from Schwann cells and DRG neurons (**Supplementary Fig. 1**).

Tace$^{-/-}$ (*Adam17*$^{-/-}$) mice die at birth[15], precluding *in vivo* analysis of myelination. To determine the role of TACE in myelin formation, we first knocked down its expression using specific short hairpin RNA (shRNA)-encoding lentiviruses. For our studies, we used three different shRNA clones (TRCN0000031949, TRCN0000031952 and TRCN0000031953) that were obtained from the RNAi Consortium (Boston, Massachusetts, USA) together with a lentiviral vector expressing a scrambled artificial sequence as a negative control. Database searches confirmed that the sequence used in the scrambled shRNA did not recognize any mammalian DNA. To validate the specificity of *Tace*-targeting shRNAs, we tested their ability to modulate the cleavage of p75^{NTR} and Notch1. Both molecules are important in myelination[16,17], but only p75^{NTR} is cleaved by TACE[18], whereas Notch1 is extracellularly processed by ADAM10 (refs. 19,20). As expected, we observed impaired p75^{NTR} cleavage in Schwann cell–DRG neuron cocultures infected with lentiviruses encoding *Tace* shRNAs, but the amount of Notch1 intracellular domain (NICD) was unaltered (**Supplementary Fig. 2**).

To corroborate the efficacy of knockdown, we infected primary rat Schwann cells for 2 d and then analyzed expression by western blotting on an Odyssey imaging system (**Fig. 1a**). All three tested shRNAs significantly decreased TACE expression by approximately 80% when compared with mock-infected or control uninfected Schwann cells (**Fig. 1b**). We then infected mouse DRG explant cultures, which contain a mix of Schwann cells and DRG neurons, with lentiviruses encoding *Tace* shRNA or a scrambled shRNA for 48 h. The cultures were grown without antimitotic agents to allow infection of both neurons and Schwann cells. Western blots confirmed effective TACE knockdown of infected cultures (data not shown). Myelination was induced by supplementing the cultures with 50 μg ml^{-1} ascorbic acid. Immunofluorescence analyses (**Fig. 1**) for myelin basic protein (MBP) and neurofilament showed that myelination was significantly greater in *Tace* shRNA–infected cultures and was already substantial 3 d after the addition of ascorbic acid. Thus, myelination in cocultures infected with *Tace* shRNA was greater and commenced earlier than myelination in scrambled shRNA–infected or control uninfected cultures, suggesting that TACE inhibits myelination. To further confirm this result, we counted the number of MBP-positive segments 3 d after ascorbic acid addition in *Tace* shRNA-infected versus uninfected or scrambled shRNA–infected cultures. Specific knockdown of *Tace* led to an approximately 15-fold increase in myelination (**Fig. 1c**). Western blotting for myelin proteins confirmed the hypermyelination. Fourteen days after the induction of myelination, myelin protein zero (MPZ) was appreciably upregulated in cocultures infected with lentiviruses encoding *Tace* shRNA (**Fig. 1d**). As *Tace* knockdown resulted in enhanced and precocious myelination, our data suggest that TACE controls the temporal activation of the myelinating program.

TACE activity *in vitro* is neuron-autonomous

These results indicate that TACE negatively controls myelination. As both Schwann cells and DRG neurons express TACE, we sought to determine whether these effects are specific to Schwann cells, neurons or both using a purified myelinating coculture system. We first infected mouse DRG neurons with lentiviruses encoding *Tace* shRNA or, as a control, with lentiviruses encoding scrambled shRNA. We then cultured these neurons with primary uninfected rat Schwann cells and induced myelination for 15 d by ascorbic acid addition; cultures were then stained for MBP and neurofilament. In comparison with control neurons, DRG neurons that were knocked down for *Tace* were substantially hypermyelinated (**Fig. 2a** and **Supplementary Fig. 3a**), and the

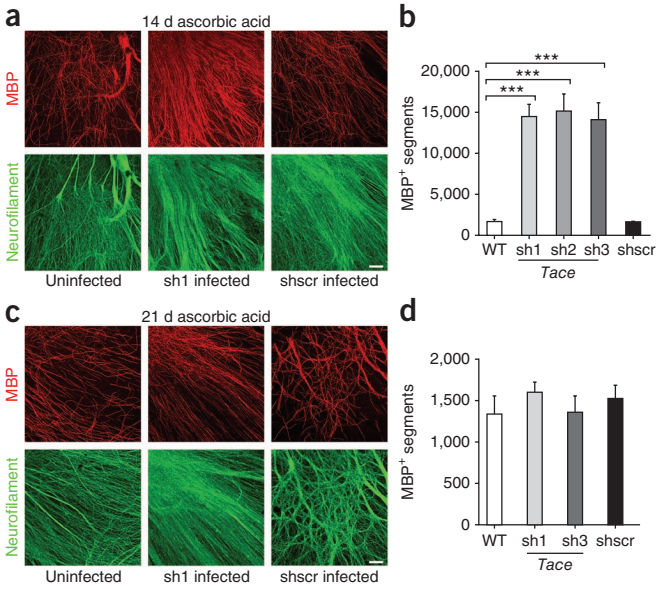

Figure 2 *In vitro* hypermyelination is neuron-autonomous. (**a**) Cocultures of mouse neurons infected with *Tace*-specific shRNA (sh1) or a scrambled artificial sequence shRNA (shscr), rid of endogenous Schwann cells and repopulated with wild-type, uninfected rat Schwann cells, were maintained in myelinating conditions for 14 d and then stained for MBP (rhodamine) and neurofilament (fluorescein). Numerous myelin segments are evident in sh1-infected cultures and fewer in uninfected (WT) and shscr-infected cultures. Scale bar, 100 µm. (**b**) Quantification of MBP$^+$ segments 14 d after the induction of myelination in control and infected (*Tace* shRNA or shscr) neuronal cocultures. Quantification was performed on the entire culture (three coverslips per experiment). $^{***}P = 0.0002$ (WT versus sh1), $^{***}P = 0.0007$ (WT versus sh2), $^{***}P = 0.0009$ (WT versus sh3). Data shown are averages of three experiments; error bars, mean ± s.e.m. (**c**) Cocultures of wild-type, uninfected mouse DRG neurons purified of endogenous Schwann cells and repopulated with rat Schwann cells that had previously been infected with sh1 or shscr. Cultures were maintained in myelinating conditions for 21 d, and then stained for MBP (rhodamine) and neurofilament (fluorescein). No difference in myelination was observed in infected versus control cultures. Scale bar, 100 µm. (**d**) Quantification of MBP$^+$ segments 21 d after the induction of myelination in control and Schwann cells infected with *Tace* shRNA or shscr and cocultured with DRG neurons. Quantification was performed on the entire culture (three coverslips per experiment, for three experiments; *P* was not significant).

number of myelinated segments in these neurons was approximately eightfold higher than the number in control neurons (**Fig. 2b**). We did not observe any effect on neurite outgrowth. We confirmed these results with western blots of MBP, myelin-associated glycoprotein (MAG) and neurofilament expression. As expected, the expression of myelin proteins was notably upregulated in the lysates of cocultures that were ablated for neuronal *Tace* (data not shown).

In a parallel set of experiments, we inactivated *Tace* in rat primary Schwann cells and cultured them with purified uninfected mouse DRG neurons. Cultures were maintained in myelinating conditions for 21 d. Immunofluorescence for MBP and neurofilament (**Fig. 2c** and **Supplementary Fig. 3b**) and western blots for MBP and MAG (data not shown) indicated that inactivation of *Tace* in Schwann cells did not enhance myelination, strongly suggesting that the inhibitory role of TACE in myelination is neuronal cell–autonomous. These results were further confirmed by assessing the numbers of MBP-positive segments in these cultures, which were comparable between *Tace* knockdown and control cultures (**Fig. 2d**). Thus, these studies indicate that TACE acts in a neuron-autonomous manner to inhibit myelination in an *in vitro* model of PNS myelination.

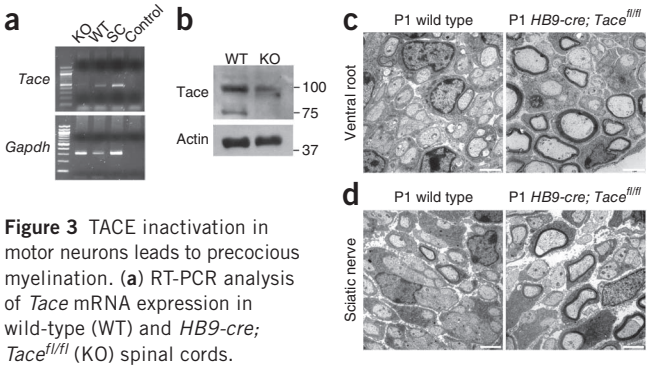

Figure 3 TACE inactivation in motor neurons leads to precocious myelination. (**a**) RT-PCR analysis of *Tace* mRNA expression in wild-type (WT) and *HB9-cre; Tace$^{fl/fl}$* (KO) spinal cords. Schwann cell mRNA (SC) was used as a positive control. *Gapdh* expression was a control for amplification. (**b**) Lysates of wild-type and *HB9-cre; Tace$^{fl/fl}$* P30 femoral nerves were fractionated by SDS-PAGE and blotted with antibodies to TACE and to actin as a loading control. TACE expression was lower in *HB9-cre; Tace$^{fl/fl}$* femoral nerve extracts than in wild-type extracts. (**c**) Electron micrographs of P1 ventral roots from wild-type and *HB9-cre; Tace$^{fl/fl}$* mice. In *HB9-cre; Tace$^{fl/fl}$* mice, fibers are hypermyelinated as compared with controls. Scale bars, 2 µm. (**d**) Electron micrographs of P1 sciatic nerves from wild-type and *HB9-cre; Tace$^{fl/fl}$* mice; most fibers in *HB9-cre; Tace$^{fl/fl}$* mice were sorted, and many were already myelinated. Scale bars, 2 µm.

In vivo inactivation of axonal TACE causes hypermyelination

To evaluate the role of TACE in myelination during development and to determine whether neuronal TACE also inhibits myelination *in vivo*, we generated transgenic mice that lack TACE specifically in motor neurons. To this end, we crossed mice containing *loxP* sites flanking exon 2 of *Tace* ('floxed' *Tace*; *Tace$^{fl/fl}$*)[21] with the *HB9-cre* transgenic line, which has been used in previous studies to drive motor neuron-specific recombination using the promoter of the *Mnx1* gene[22]. Ablation of *Tace* exon 2 leads to a functional null protein[21]. We screened the genotype by PCR analysis of genomic DNA that was prepared from the tail and spinal cord of *HB9-cre; Tace$^{fl/fl}$* and wild-type controls (data not shown). As the *HB9-cre* transgene is expressed in motor neurons, we corroborated efficient recombination by determining *Tace* mRNA expression using RT-PCR on spinal cord of *HB9-cre; Tace$^{fl/fl}$* and wild-type mice (**Fig. 3a**). We also assessed TACE protein amounts in lysates that were prepared from postnatal day (P) 30 wild-type and *HB9-cre; Tace$^{fl/fl}$* femoral nerves (**Fig. 3b**). TACE expression was lower both at the mRNA and protein levels in *HB9-cre; Tace$^{fl/fl}$* mice. Residual expression was probably due to un-recombined *Tace* that was present in other cells; in femoral nerves, these cells would be mainly Schwann cells and sensory nerve fibers.

Ultrastructural analysis of the ventral roots and sciatic nerves from newborn (P1) *HB9-cre; Tace$^{fl/fl}$* mice showed that the onset of myelination in the ventral roots of these mice was accelerated (**Fig. 3c**). As expected, we observed that some fibers in P1 sciatic nerves, which contain both sensory and motor fibers, were hypermyelinated (**Fig. 3d**). Quantification of the number of myelinated fibers demonstrated that there were significantly more in *HB9-cre; Tace$^{fl/fl}$* mice ($P = 0.0039$); the total number of nerve fibers was similar in both genotypes (**Supplementary Table 1**).

To evaluate whether the hypermyelination of *HB9-cre; Tace$^{fl/fl}$* mice is maintained during active phases of myelination, we analyzed peripheral nerve morphology in P7 and P15 sciatic nerves. At both time points, neurites were hypermyelinated, as evidenced in semi-thin sections (**Fig. 4a**,**b**, top panels) and in electron micrographs

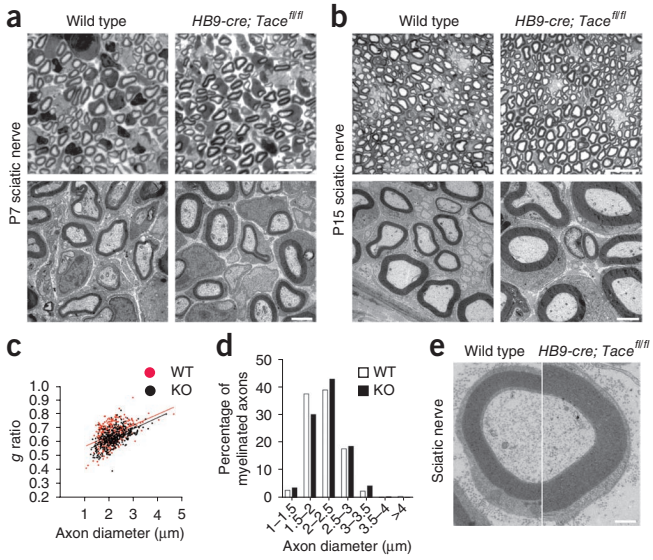

Figure 4 *HB9-cre; Tace*$^{fl/fl}$ mice are hypermyelinated during development. (**a**) Semithin sections (top panels) and electron micrographs (bottom panels) of wild-type and *HB9-cre; Tace*$^{fl/fl}$ P7 nerves. Scale bars, 15 μm (top panels) and 2 μm (bottom panels). (**b**) Semithin sections (top panels) and electron micrographs (bottom panels) of wild-type and *HB9-cre; Tace*$^{fl/fl}$ P15 nerves. Scale bars, 20 μm (top panels) and 2 μm (bottom panels). (**c**) *g* ratios as a function of axon diameter were significantly different between wild-type (WT) P7 mice and *HB9-cre; Tace*$^{fl/fl}$ (KO) P7 mice ($P = 0.0007$). The graph represents the *g* ratios obtained from more than 500 myelinated axons per genotype (a total of three mice per genotype). (**d**) The distribution of myelinated fibers was similar in *HB9-cre; Tace*$^{fl/fl}$ and wild-type P7 sciatic nerves (*P* was not significant). (**e**) Myelinated axons of similar diameters demonstrate that myelin in wild-type versus *HB9-cre; Tace*$^{fl/fl}$ sciatic nerves had identical periodicity but differed considerably in the number of lamellae. Scale bar, 500 nm.

(**Fig. 4a**,**b**, lower panels). The hypermyelinating phenotype was also confirmed by *g* ratio (axon diameter/fiber diameter) measurements (**Fig. 4c**), which showed that the *g* ratio of P7 fibers of sciatic nerves was significantly lower in *HB9-cre; Tace*$^{fl/fl}$ mice than in wild-type mice (**Supplementary Table 1**). This change did not result in altered fiber diameters in *HB9-cre; Tace*$^{fl/fl}$, which were similar to those of wild-type mice (**Fig. 4d**), strongly suggesting that the observed phenotype is due to changes in the myelin sheath. As suggested from our previous data, hypermyelination in *HB9-cre; Tace*$^{fl/fl}$ mice resulted in considerably more myelin lamellae surrounding fibers of similar caliber, with no alteration to myelin periodicity (**Fig. 4e**).

Morphological and ultrastructural analysis of P30 *HB9-cre; Tace*$^{fl/fl}$ ventral roots (**Fig. 5a**) and sciatic nerves (**Fig. 5b**) and *g* ratio measurements in sciatic nerves (**Fig. 5** and **Supplementary Table 1**) confirmed hypermyelination in adult mice, strongly suggesting that this effect is maintained throughout development. Unexpectedly, we observed a significant number of myelinated fibers with axons of less than 1 μm diameter and markedly smaller axonal diameters for myelinated fibers in sciatic nerves of *HB9-cre; Tace*$^{fl/fl}$, despite the total number of myelinated fibers being similar between genotypes (wild type, 1,717; *HB9-cre; Tace*$^{fl/fl}$, 1,697) (**Fig. 5g** and **Supplementary Table 1**). Whether this difference is due to ectopic myelination or constriction of axonal caliber will require further investigation. Nonetheless, this alteration is unlikely to explain the hypermyelination, as both *in vitro* and *in vivo* studies indicate that axonal diameter increases with myelin formation[23,24]. Of note, we similarly observed myelin sheath surrounding several fibers whose diameter was less than 1 μm in ventral roots of *HB9-cre; Tace*$^{fl/fl}$

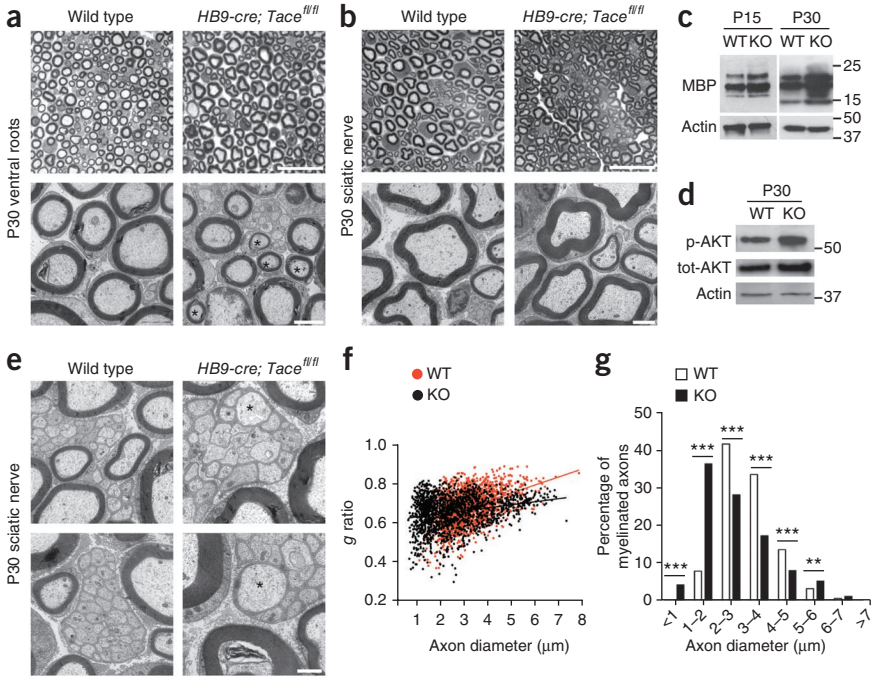

Figure 5 *HB9-cre; Tace*$^{fl/fl}$ adult mice were hypermyelinated and Remak fibers were aberrantly ensheathed. (**a**) Semithin sections (top panels) and electron micrographs (bottom panels) of wild-type and *HB9-cre; Tace*$^{fl/fl}$ P30 ventral roots. Scale bars, 20 μm (top panels) and 2 μm (bottom panels). Asterisks indicate heavily myelinated fibers of less than 1 μm diameter. (**b**) Semithin sections (top panels) and electron micrographs (bottom panels) of wild-type and *HB9-cre; Tace*$^{fl/fl}$ P30 sciatic nerves. Scale bars, 20 μm (top panels) and 2 μm (bottom panels). (**c**) Lysates of wild-type (WT) and *HB9-cre; Tace*$^{fl/fl}$ (KO) P15 and P30 femoral nerves were blotted with antibodies to MBP and to actin as a loading control. MBP expression was upregulated in femoral nerve extracts from *HB9-cre; Tace*$^{fl/fl}$ mice. (**d**) Lysates of wild-type and *HB9-cre; Tace*$^{fl/fl}$ P30 femoral nerves were blotted with antibodies to p-AKT, total AKT (tot-AKT) and actin as a loading control. p-AKT expression was notably upregulated in *HB9-cre; Tace*$^{fl/fl}$ femoral nerve extracts. (**e**) Impaired sorting of Remak fibers of *HB9-cre; Tace*$^{fl/fl}$ sciatic nerves. In wild-type mice, unmyelinated axons are segregated into separate pockets of Remak bundles and fully wrapped by Schwann cells. In *HB9-cre; Tace*$^{fl/fl}$ mice, Remak bundles contained abnormally large-caliber axons (asterisks), and Schwann cells failed to ensheath the axons. Scale bar, 1 μm. (**f**) Significant difference in *g* ratios as a function of axon diameter between P30 sciatic nerve fibers from wild-type and *HB9-cre; Tace*$^{fl/fl}$ mice ($P < 0.0001$). The graph represents the *g* ratio obtained from more than 700 myelinated axons (three mice per genotype). (**g**) Myelinated axons in *HB9-cre; Tace*$^{fl/fl}$ P30 sciatic nerves were significantly smaller (***$P < 0.0001$, **$P = 0.0051$). Approximately 7% of myelinated fibers were <1 μm in diameter in *HB9-cre; Tace*$^{fl/fl}$ sciatic nerves. In each genotype, we counted >700 axons in a total of three mice. Error bars, mean ± s.e.m.

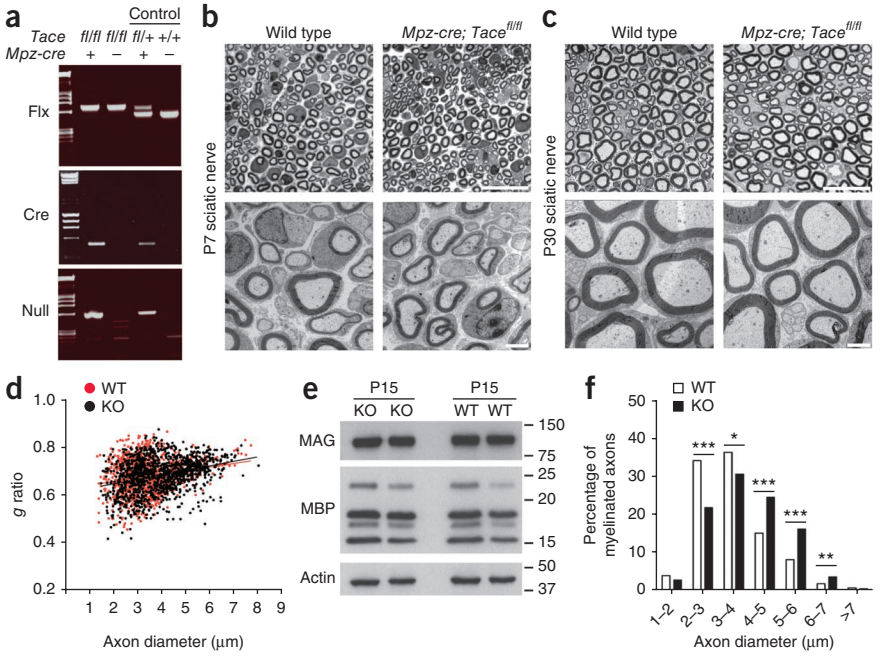

Figure 6 *Mpz-cre; Tace*$^{fl/fl}$ mice were normally myelinated. (**a**) Genotyping PCR on genomic DNA prepared from sciatic nerves of P15 wild-type (+/+) and *Mpz-cre; Tace*$^{fl/fl}$ mice. Tace recombination was present in nerves of *Tace*$^{fl/fl}$ mice expressing the Cre recombinase also. Flx, amplification of the *fl* allele; Cre, amplification of *cre*; null, amplification of the recombined allele[21]. (**b**) *Mpz-cre; Tace*$^{fl/fl}$ mice had a comparable myelin thickness to wild-type mice. Semithin sections (top panels) and electron micrographs (bottom panels) of wild-type and *Mpz-cre; Tace*$^{fl/fl}$ P7 sciatic nerves. Scale bars, 20 μm (top panels) and 2 μm (bottom panels). (**c**) Semithin sections (top panels) and electron micrographs (bottom panels) of wild-type and *Mpz-cre; Tace*$^{fl/fl}$ P30 sciatic nerves. Scale bars, 20 μm (top panels) and 2 μm (bottom panels). (**d**) *g* ratios as a function of axon diameter were identical in wild-type (WT) and *Mpz-cre; Tace*$^{fl/fl}$ (KO) P30 sciatic nerve fibers (*P* was not significant). The graph represents the *g* ratios obtained from >300 myelinated axons (three mice per genotype). (**e**) Lysates of wild-type and *Mpz-cre; Tace*$^{fl/fl}$ P15 sciatic nerves were fractionated by SDS-PAGE and blotted with antibodies to myelin proteins (MAG and MBP) and to actin as a loading control. No alteration in myelin protein expression was observed among wild-type and *Mpz-cre; Tace*$^{fl/fl}$ mice. (**f**) *Mpz-cre; Tace*$^{fl/fl}$ mice have a slightly but significantly greater axonal diameters than wild-type mice (* $P < 0.036$, ** $P < 0.001$, *** $P < 0.0001$). Myelinated axons of P30 sciatic nerves were binned based on their axonal diameters. >1,200 axons were counted from three different mice per genotype. Error bars, mean ± s.e.m.

(**Fig. 5a**, asterisks). To determine whether the myelin protein content parallels the hypermyelinating phenotype, we checked MBP expression in P15 and P30 femoral nerves of wild-type and *HB9-cre; Tace*$^{fl/fl}$ by Western blotting. As expected, hypermyelination was accompanied by higher MBP expression (**Fig. 5c**). Of note, even amounts of phosphorylated AKT (p-AKT) (**Fig. 5d**)—a key effector of the PI3K pathway, which acts downstream of NRG1 type III[1] and is important for PNS myelination[25,26]—were higher in P30 femoral nerves of *HB9-cre; Tace*$^{fl/fl}$ mice than in those of wild-type mice.

Our ultrastructural analysis also showed that ablation of neuronal *Tace* altered the organization of C fibers, which are engulfed by non-myelinated Schwann cells in Remak bundles. In fact, we observed unsorted and unmyelinated fibers that were larger than 1 μm in diameter in *HB9-cre; Tace*$^{fl/fl}$ Remak bundles (**Fig. 5e**, asterisks), suggesting an impaired sorting process. Furthermore, in many cases Remak bundles lacked intervening Schwann cell processes, suggesting that TACE also affects the ensheathment process of non-myelinated fibers.

To test whether TACE haploinsufficiency induces hypermyelination, we generated a complete *Tace*$^{+/-}$ transgenic line by crossing *Tace*$^{fl/fl}$ mice with mice with a *CMV-cre* transgene that drives recombination in all cells[27]. Morphological analysis, *g* ratio measurements and western blotting for myelin proteins showed that *Tace*$^{+/-}$ P30 sciatic nerves were myelinated normally, indicating that residual TACE activity is sufficient to regulate myelin formation (**Supplementary Fig. 4** and **Supplementary Table 1**).

Only axonal TACE determines hypermyelination

To corroborate our previous results, which indicate that hypermyelination is due to a neuronal cell–autonomous mechanism, we deleted *Tace* in Schwann cells *in vivo* by crossing *Tace*-floxed transgenic mice with a *Mpz-cre* transgenic line (creating *Mpz-cre; Tace*$^{fl/fl}$ mice)[28]. We confirmed efficient recombination in genomic DNA of P15 sciatic nerves of *Mpz-cre; Tace*$^{fl/fl}$ mice by PCR analyses (**Fig. 6a**). Myelination in P7 and P30 *Mpz-cre; Tace*$^{fl/fl}$ sciatic nerves was similar to that of wild-type control mice, as assessed by semithin sections (top panels in **Fig. 6b**,**c**) and ultrastructural analysis (lower panels in **Fig. 6b**,**c**). This result was further confirmed by *g* ratio measurements (**Fig. 6d**), which were not significantly different in wild-type and *Mpz-cre; Tace*$^{fl/fl}$ mice (**Supplementary Table 1**). Furthermore, MBP and MAG protein levels were similar in lysates of wild-type and *Mpz-cre; Tace*$^{fl/fl}$ P15 sciatic nerves (**Fig. 6e**). Surprisingly, despite the similar numbers of myelinated fibers in wild-type and *Mpz-cre; Tace*$^{fl/fl}$ mice (wild type, 1,298; *Mpz-cre; Tace*$^{fl/fl}$, 1,244), axonal diameters were slightly greater in *Mpz-cre; Tace*$^{fl/fl}$ sciatic nerves (**Fig. 6f** and **Supplementary Table 1**). Furthermore, the myelinated fibers of *Mpz-cre; Tace*$^{fl/fl}$ mice had more periaxonal space and an accumulation of organelles in the inner cytoplasmic collar (**Supplementary Fig. 5**), suggesting that glial TACE may process molecules that are implicated in myelin compaction and/or adhesion.

Taken together, these *in vivo* analyses provide compelling evidence that neuronal TACE inhibits myelination in a cell-autonomous mechanism. Ablation of *Tace* in motor neurons accelerates the myelination process and results in hypermyelination, leading to a greater number of myelin lamellae than in wild-type fibers with similar caliber, and ectopic myelination of small-caliber fibers that would normally be unmyelinated. In addition, our findings indicate that glial TACE also participates in the myelinating process, although it does not regulate myelin thickness.

TACE cleaves NRG1 and controls axonal NRG1 type III levels

The phenotype observed in *HB9-cre; Tace*$^{fl/fl}$ mice, particularly the greater number of myelin lamellae *in vivo*, strongly resembles the hypermyelinating phenotype of mice overexpressing NRG1 type III[2]. In addition, ablation of *Tace* is sufficient to determine myelination of fibers that would normally be amyelinated, mirroring what happens when NRG1 type III is ectopically expressed[1]. Thus, by cleaving NRG1 (ref. 13), TACE might regulate the amount of axonal NRG1 type III and, hence, PNS myelination. To determine whether NRG1 shedding is altered in the absence of TACE, we analyzed NRG1 expression in

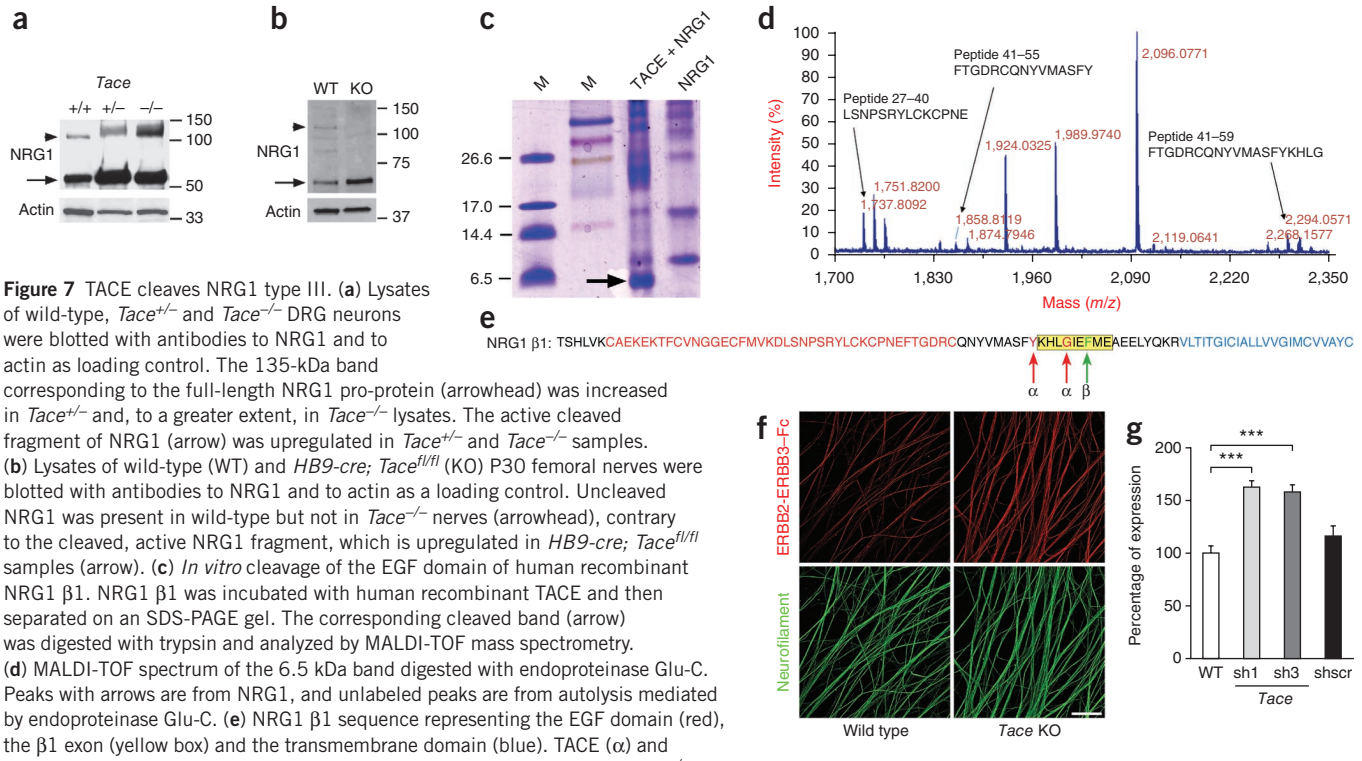

Figure 7 TACE cleaves NRG1 type III. (**a**) Lysates of wild-type, *Tace*$^{+/-}$ and *Tace*$^{-/-}$ DRG neurons were blotted with antibodies to NRG1 and to actin as loading control. The 135-kDa band corresponding to the full-length NRG1 pro-protein (arrowhead) was increased in *Tace*$^{+/-}$ and, to a greater extent, in *Tace*$^{-/-}$ lysates. The active cleaved fragment of NRG1 (arrow) was upregulated in *Tace*$^{+/-}$ and *Tace*$^{-/-}$ samples. (**b**) Lysates of wild-type (WT) and *HB9-cre; Tace*$^{fl/fl}$ (KO) P30 femoral nerves were blotted with antibodies to NRG1 and to actin as a loading control. Uncleaved NRG1 was present in wild-type but not in *Tace*$^{-/-}$ nerves (arrowhead), contrary to the cleaved, active NRG1 fragment, which is upregulated in *HB9-cre; Tace*$^{fl/fl}$ samples (arrow). (**c**) *In vitro* cleavage of the EGF domain of human recombinant NRG1 β1. NRG1 β1 was incubated with human recombinant TACE and then separated on an SDS-PAGE gel. The corresponding cleaved band (arrow) was digested with trypsin and analyzed by MALDI-TOF mass spectrometry. (**d**) MALDI-TOF spectrum of the 6.5 kDa band digested with endoproteinase Glu-C. Peaks with arrows are from NRG1, and unlabeled peaks are from autolysis mediated by endoproteinase Glu-C. (**e**) NRG1 β1 sequence representing the EGF domain (red), the β1 exon (yellow box) and the transmembrane domain (blue). TACE (α) and BACE1 (β) cleavage sites are also indicated. (**f**) Cultures of wild-type and *Tace*$^{-/-}$ DRG neurons were incubated with ERBB2-ERBB3–Fc and the binding visualized with rhodamine-conjugated antibodies to human Fc (rhodamine); neurofilament staining from corresponding fields is shown (fluorescein). Scale bar, 50 μm. (**g**) Quantification of the ERBB2-ERBB3 binding signal. Quantification was performed on confocal images that were acquired with the same z-stack and laser intensity (a total of five coverslips per experiment, for three experiments). ***$P < 0.0001$. Error bars, mean ± s.e.m.

lysates of wild-type, *Tace*$^{+/-}$ and *Tace*$^{-/-}$ DRG neurons prepared from embryonic day 14.5 embryos (**Fig. 7a**) and in lysates of P30 *HB9-cre; Tace*$^{fl/fl}$ femoral nerves (**Fig. 7b**). In the absence of TACE, NRG1 processing was impaired, as there was more of the unprocessed pro-protein form in *HB9-cre; Tace*$^{fl/fl}$ DRG neurons. Of note, unprocessed NRG1 pro-protein was absent in *HB9-cre; Tace*$^{fl/fl}$ femoral nerves and barely present in wild-type control extracts. This difference is likely to be due to altered NRG1 expression in DRG neurons in culture and in sciatic nerves[1]. More importantly, the amount of cleaved NRG1 was similarly greater in the absence of TACE, probably owing to enhanced activity of other secretases (such as BACE1).

To further confirm these data, we mapped the TACE cleavage site of NRG1 by mass spectrometry. To this end, we incubated 2 μg of human recombinant NRG1 containing the EGF β-exon domain (NRG β1), the most abundant NRG1 isoform expressed in the nervous system, with 1 μg of human recombinant TACE. The proteins were then separated on a Tris-tricine gel (to favor the resolution of low-molecular-mass bands) together with native, uncleaved recombinant NRG1 β1 for comparison (**Fig. 7c**). The reaction generated a cleavage product of ~6 kDa, which was digested with endoproteinase Glu-C and analyzed by matrix-assisted laser desorption/ionization–time of flight (MALDI-TOF) mass spectrometry. In the MALDI-TOF spectrum, two potential C-terminal peptides were detected that did not correspond to endoproteinase Glu-C cleavage (**Supplementary Fig. 6**) and therefore derived from TACE activity (**Fig. 7d**). These peptides, with masses of 1,858.812 Da and 2,294.057 Da, corresponded to the peptide sequences FTGDRCQNYVMASFY and FTGDRCQNYVMASFYKHLG, respectively, suggesting that TACE cleaves NRG1 β1 either upstream or in the β-exon of the EGF domain, 3–6 amino acids before the previously identified BACE1 site (**Fig. 7e**)[4]. In our analysis, we did not observe cleavage at the BACE1 site of NRG1.

To determine whether the activity of NRG1 type III is altered following TACE cleavage, we incubated wild-type, control and *Tace*$^{-/-}$ DRG neurons, obtained by crossing *Tace*$^{+/-}$ mice, with the receptor ERBB2-ERBB3 fused to the Fc portion of human immunoglobulin G (ERBB2-ERBB3–Fc); this chimeric protein binds to NRG1 type III molecules, the only NRG1 molecules that are expressed on the axonal surface[1]. Chimeric ERBB2-ERBB3–Fc bound more robustly to DRG neurons lacking TACE than to wild-type uninfected or control-shRNA-infected DRG neurons (**Fig. 7f**). Similar results were obtained in DRG neurons in which *Tace* expression had been ablated by shRNA infection (**Supplementary Fig. 7**). Inhibition of *Tace* expression resulted in an ~50% increase in the amount of NRG1 type III on the axonal surface (**Fig. 7g**). These results confirm that TACE cleaves NRG1 and suggest that TACE inhibits myelination by limiting the amount of functional NRG1 type III on the axonal surface.

TACE alters NRG1 type III signaling and myelination

Despite the key role of NRG1 type III in myelination, this is not the sole NRG1 isoform to be expressed by DRG neurons. In particular, DRG neurons also express NRG1 type I[29], which is also processed by α-secretases[1] and has an amino acid sequence that is identical to that of NRG1 type III in the region cleaved by TACE. Thus, TACE could affect myelination by inhibiting the processing of NRG1 type I. Similarly, TACE could process other molecules that regulate myelin formation.

To further investigate the role of TACE-specific processing of NRG1 type III, we downregulated TACE activity in neurons in which the NRG1 type III isoform was disrupted (*Nrg1 type III*$^{-/-}$ neurons) (**Supplementary Fig. 8b**) and investigated whether ablation of *Tace* could rescue myelination in these neurons[1]. We infected *Nrg1* type III$^{-/-}$ DRG neurons with *Tace*-specific shRNA or with a scrambled shRNA control and rid

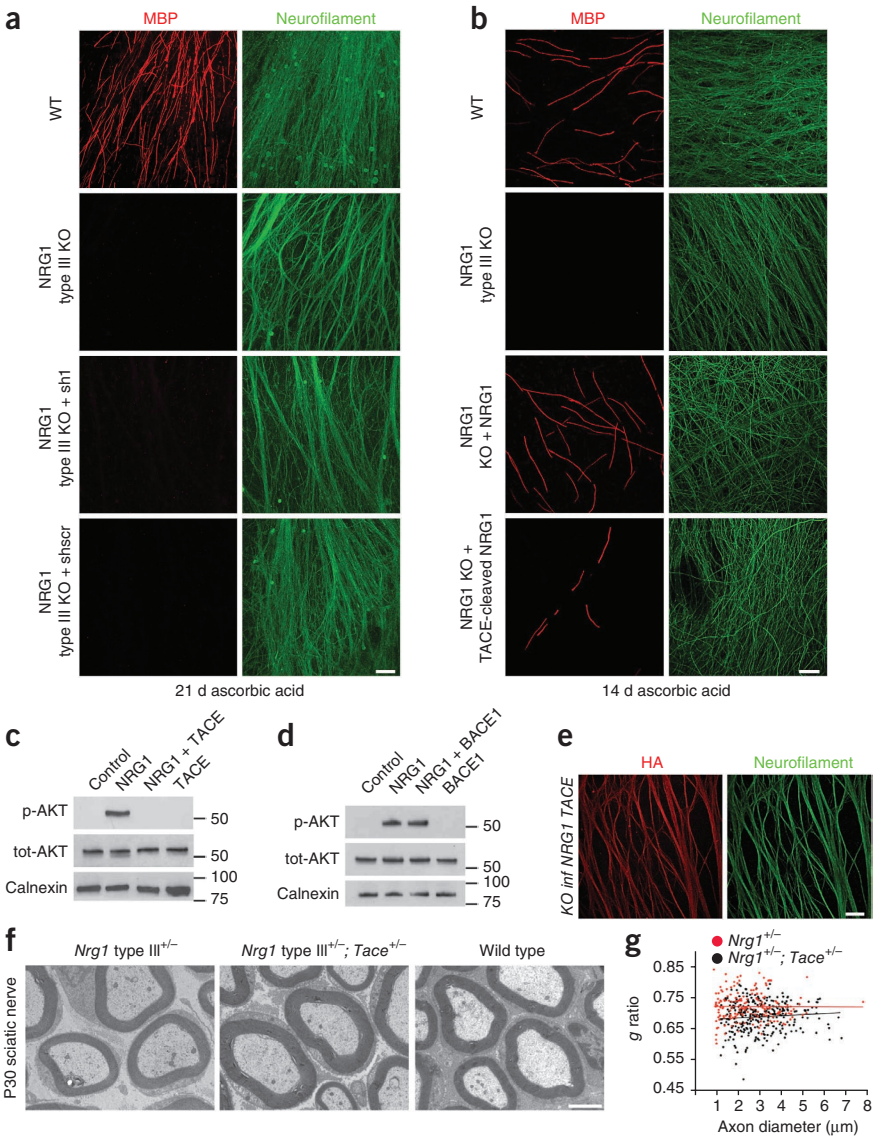

Figure 8 TACE regulates NRG1 type III activity. (**a**) Cocultures of wild-type (WT) and *Nrg1 type III*$^{-/-}$ (KO) DRG neurons that were uninfected or infected with *Tace*-specific shRNA (sh1) or scrambled shRNA (shscr) were maintained in myelinating conditions with rat Schwann cells for 21 d and then stained for MBP (rhodamine) and neurofilament (fluorescein). *Tace* knockdown does not rescue myelination in *Nrg1 type III*$^{-/-}$ neurons. Scale bar, 50 μm. (**b**) Cocultures of wild-type or *Nrg1 type III*$^{-/-}$ DRG neurons were uninfected or infected with full-length NRG1 type III or NRG1 cleaved at the TACE cleavage site. These cocultures were maintained in myelinating conditions with wild-type rat Schwann cells for 14 d, fixed and stained for MBP (rhodamine) and neurofilament (fluorescein). NRG1 cleaved by TACE inefficiently rescued myelination in *Nrg1 type III*$^{-/-}$ neurons. The few MBP-positive segments observed (nine coverslips from three experiments) are shown. Scale bar, 50 μm. (**c**) Rat primary Schwann cells were starved for 16 h and not stimulated (control) or stimulated with 50 ng ml^{-1} NRG1 β1 (NRG1), 50 ng ml^{-1} NRG1 β1 cleaved by TACE (NRG1 + TACE) or 50 ng ml^{-1} TACE alone (TACE). Lysates of these cells were blotted with antibodies to p-AKT, total AKT (tot-AKT) and calnexin as a loading control. (**d**) Rat primary Schwann cells were starved for 16 h and not stimulated (control) or stimulated with 50 ng ml^{-1} NRG1 β1 (NRG1), 50 ng ml^{-1} NRG1 β1 cleaved by BACE1 (NRG1+BACE1) or 50 ng ml^{-1} BACE1 alone (BACE1). Lysates from these cells were blotted with antibodies to p-AKT, total AKT and calnexin as a loading control. (**e**) NRG1 cleaved by TACE was detected on the axonal surface of *Nrg1 type III*$^{-/-}$ neurons infected with lentiviruses expressing NRG1 processed at the TACE cleavage site by live staining for the NRG1 hemagglutinin (HA) epitope (rhodamine) and neurofilament (fluorescein). Scale bar, 50 μm. (**f**) Electron micrographs of *NRG1* type III$^{+/-}$, *NRG1* type III$^{+/-}$; *Tace*$^{+/-}$ and wild-type P30 sciatic nerves. *NRG1* type III$^{+/-}$; *Tace*$^{+/-}$ fibers are normally myelinated. Scale bar, 2 μm. (**g**) *g* ratios of P30 sciatic nerve fibers as a function of axon diameter were lower in *NRG1* type III$^{+/-}$; *Tace*$^{+/-}$ mice than in *NRG1* type III$^{+/-}$ mice ($P < 0.0001$). The graph represents the *g* ratios obtained from >200 myelinated axons (three mice per genotype).

the cultures of endogenous Schwann cells and fibroblasts (**Fig. 8** and **Supplementary Fig. 8a**). We then repopulated the neurons with rat primary Schwann cells and, 21 d after the induction of myelination, we examined MBP and neurofilament expression by immunofluorescence (**Fig. 8a**) and western blot (**Supplementary Fig. 8c**) analyses. Ablation of *Tace* in *Nrg1 type III*$^{-/-}$ neurons did not rescue myelination (**Fig. 8**).

As PI3K is a key effector of NRG1 signaling and myelination, we tested whether NRG1 cleaved by TACE or BACE1 modulated this pathway. Thus, we incubated NRG1 β1 with recombinant human TACE or BACE1 and determined p-AKT activation in starved primary rat Schwann cells. Importantly, TACE-cleaved NRG1 did not activate p-AKT (**Fig. 8c**), unlike BACE1-cleaved NRG1 (**Fig. 8d**). This result suggests that TACE and BACE1 differentially activate NRG1, leading to either impairment (TACE) or activation (BACE1) of PI3K signaling and, hence, of myelination in Schwann cells. Furthermore, unlike a lentiviral construct expressing full-length NRG1 type III, a lentiviral construct expressing a cDNA encoding the portion of NRG1 type III from the N terminus to the histidine located between the identified TACE cleavage sites (**Fig 7e**), rescued myelination of *Nrg1 type III*$^{-/-}$ DRGs inefficiently (**Fig. 8b**), despite being expressed on the axonal surface (**Fig. 8e**).

To further confirm the inhibitory role of TACE on NRG1 type III, we tested whether a cross with *Tace*$^{+/-}$ mice, whose neurons are myelinated normally, would rescue hypomyelination of *Nrg1 type III*$^{+/-}$ mice. Morphological analysis of compound *Nrg1 type III*$^{+/-}$; *Tace*$^{+/-}$ P30 sciatic nerves (**Fig. 8f**) and *g* ratio measurements (**Fig. 8g** and **Supplementary Table 1**) showed that a 50% reduction in TACE activity was sufficient to rescue myelination in *Nrg1 type III*$^{+/-}$ mice.

Taken together, these results provide strong evidence that TACE inhibits myelination by modulating the amount of functional NRG1 type III on axonal membranes. They also describe a newly discovered level of regulation of PNS myelination.

DISCUSSION

In this study, we describe a previously uncharacterized inhibitory mechanism that regulates the extent of myelination in the PNS. As

myelin is required for the correct transmission of electrical impulses along axons and for the preservation of axonal integrity, understanding the processes that direct myelin formation and assembly is important for the development of effective treatments for demyelinating diseases. Using TACE knockdown strategies *in vitro* and conditional inactivation of TACE *in vivo*, we show that this inhibitory role is neuron-autonomous. We further demonstrate that TACE activity regulates NRG1 type III processing on axons and modulates the PI3K pathway in Schwann cells, thereby ensuring the correct timing and and myelination levels of PNS axons. These results underscore the existence of several components that control myelination and, to our knowledge, represent the first example of a negative control of myelination by secretases.

Several secretases have previously been implicated in regulating myelination. Among these, only BACE1 (refs. 3,5) and the zinc peptidase nardylisin (NRD1)[30] have been directly linked to NRG1 type III cleavage; both positively regulate myelination. Biochemical studies have shown that BACE1 cleaves NRG1 type III[4]. As *Bace1*$^{-/-}$ mice are hypomyelinated in the CNS[5] and PNS[3], similarly to *NRG1 type III*$^{+/-}$ mice[1,2], BACE1 cleavage should activate NRG1 type III. NRD1 was originally identified as an enhancer of the activity of ADAM proteases, including TACE[30]. However, *Nrd1*$^{-/-}$ mice are hypomyelinated in the CNS and PNS, rather than hypermyelinated, as would be expected for a TACE hypomorph based on our results. This suggests that NRD1 may principally regulate other secretases that mediate NRG1 cleavage, including BACE1 (ref. 30). Moreover, in this study TACE was shown to mediate the cleavage of NRG1 type I[30], which we and others have shown is not involved in PNS myelination[1,2].

A key finding is that these inhibitory effects of TACE directly oppose those of BACE1 (refs. 3–5), as indicated by differential activation of the PI3K pathway in Schwann cells. TACE inactivation leads to an acceleration of the myelinating program *in vitro* and *in vivo*. Together, these data indicate that secretases provide a post-transcriptional control of the amount of functional NRG1 type III and suggest that the balance between BACE1 and TACE activity is a key determinant of the timing and extent of PNS myelination (**Supplementary Fig. 9**).

An important question is how the balance of NRG1 cleavage by these distinct secretases is regulated, including whether cleavage by one secretase precludes processing by the others. The specificity that is achieved by sheddases, which normally process multiple substrates, has not been completely clarified. Several studies have reported that secretases do not recognize a specific amino acid sequence[31]. This complexity is further enhanced by the fact that the same sheddase can process a single protein at different sites, as in the case of APP[32]. Thus, even though this is a highly conserved process, the actual mechanism by which regulated shedding occurs is unknown. Nonetheless, comparisons of the amino acid sequences of different substrates that are cleaved by the same secretase, together with the use of peptide libraries to identify putative consensus cleavage sequences, have helped in the identification of preferential amino acids that are targeted by secretases. Recent studies have reported that TACE selects small aliphatic residues immediately downstream of the cleavage site (P1′ site). Of note, for one of the cleavage sites identified by mass spectrometry, the isoleucine in the P1′ position is among the preferred amino acids for TACE cleavage[31].

The TACE cleavage site is very close to the previously identified BACE1 cleavage site of NRG1 type III[4], suggesting that the two processing sites are mutually exclusive. TACE and BACE1 frequently have common substrates, although normally the corresponding cleavage sites are not nearby[33]. TACE-mediated processing and BACE1-mediated processing of NRG1 type III most probably occur at different subcellular locations, further strengthening the possibility that that these two events are distinct. The mature form of TACE is mainly located in the perinuclear space[34] and in the plasma membrane[35]. In addition, TACE and NRG1 colocalize in lipid rafts, where they could interact[36,37]. By contrast, BACE1 is internalized from the plasma membrane to the endosomal compartments and then recycled to the late Golgi[33,38]. As NRG1 molecules are glycosylated[39], they are probably delivered to the plasma membrane through the trans-Golgi network, where they may be activated by BACE1. Whether BACE1-mediated cleavage of NRG1 type III also occurs in endosomes and determines NRG1 type III recycling or degradation, as in the case of cleavage of APP[40], is unknown. Further studies are required to establish the identity of the cellular organelles in which NRG1 type III processing occurs, as the different localization could influence NRG1 type III-mediated effects on myelination.

Our study suggests that TACE inhibits myelination by modulating NRG1 type III activity rather than total surface levels. Thus, in the absence of TACE, the active form of NRG1 was upregulated (**Fig. 7**). Our results indicate that TACE cleaves NRG1 type III in the β exon of the EGF domain, generating a nonfunctional molecule that inefficiently rescues myelination of *Nrg1 type III*$^{-/-}$ DRG neurons (**Fig. 8**). We suggest that this cleavage affects the affinity of NRG1 type III for the ERBB2-ERBB3 heterodimer, as indicated by enhanced ERBB2-ERBB3–Fc binding in the absence of TACE (**Fig. 7**). In agreement with this model, there was more p-AKT in femoral nerves of *Tace*$^{-/-}$ mice (**Fig. 5**), and NRG1 cleaved by TACE did not activate the PI3K pathway in Schwann cells (**Fig. 8**). A corollary to these findings is that nearby cleavage of NRG1 by BACE1 enhanced the affinity of NRG1 for ERBB receptors, as suggested by higher levels of AKT phosphorylation (**Fig. 8**).

The effects of TACE cleavage are neuron-autonomous. We observed the hypermyelinating phenotype only when *Tace* was ablated in neurons, further strengthening the likelihood that TACE acts on axonal NRG1 type III. More importantly, this hypermyelination closely resembled that of mice overexpressing *Nrg1 type III*$^{-/-2}$ and was due to the higher number of myelin lamellae. In addition, reduced TACE activity was sufficient to rescue myelination in *NRG1 type III*$^{+/-}$ mice. Further, ablation of neuronal *Tace* determined aberrant myelination of small-caliber axons that would normally be unmyelinated, probably by altering the threshold levels of expression of axonal NRG1 type III[1]. Finally, inhibition of TACE in *Nrg1 type III*$^{-/-}$ neurons was not enough to rescue the myelination defect of these neurons, further suggesting that TACE processes NRG1 type III. Nonetheless, we cannot exclude the possibility that TACE might act on a separate molecule that is not functional in *Nrg1 type III*$^{-/-}$ neurons because it is inactive or absent owing to the absence of NRG1 type III. A likely candidate is Notch1, an inhibitor of myelination[17], although Notch1 processing is not altered in cocultures of Schwann cells and DRG neurons infected with *Tace* shRNAs (**Supplementary Fig. 2**). In agreement, it has been shown recently that ADAM10 is the essential protease that regulates Notch1 cleavage, and does so in a ligand-dependent manner, whereas TACE participates in substrate cleavage in a ligand-independent manner[41].

Surprisingly, defects in the Remak bundles of *HB9-cre; Tace*$^{fl/fl}$ mice partially resemble those of *NRG1 type III*$^{+/-}$ mice[1]. Unlike these NRG1-haploinsufficient mice, however, *HB9-cre; Tace*$^{fl/fl}$ mice were also characterized by unsorted fibers of large diameter, suggesting that TACE cleaves a different substrate in Remak bundles. Of note, MAL-overexpressing mice[42] have similar alterations to and accumulation of p75^{NTR}, another target of TACE[6], in nonmyelinating Schwann cells. Accordingly, TACE inhibition altered the processing of p75^{NTR}. Although we cannot exclude the contribution of p75^{NTR}, it has been suggested that glia and not axonal p75^{NTR} promotes myelination *in vitro*[16] and remyelination *in vivo*[43]. That TACE might cleave molecules

other than NRG1 type III that are also implicated in myelination is also suggested by our analyses of *Mpz-cre; Tace*$^{fl/fl}$ mice and by the reductions in the caliber of myelinated fibers in *HB9-cre; Tace*$^{fl/fl}$ mice.

In summary, we describe a previously uncharacterized mechanism that controls the regulation of myelination during PNS development, by modulating a signaling pathway. Recent studies suggest that NRG1 type III is dispensable for myelin maintenance but important for remyelination[44,45]. The question of whether TACE plays a part during myelin maintenance or remyelination will require further investigations. The therapeutic potential of TACE modulation is underscored by the development of several compounds that specifically target TACE and have already been tested in clinical trials for rheumatoid arthritis[46]. Thus, TACE inhibition may be a useful strategy to promote myelination in dysmyelinating peripheral neuropathies.

METHODS

Methods and any associated references are available in the online version of the paper at http://www.nature.com/natureneuroscience/.

Note: Supplementary information is available on the Nature Neuroscience website.

ACKNOWLEDGMENTS

We thank S. Arber (University of Basel) for providing the *HB9-cre* transgenic line, M. Filbin (Hunter College) for antibodies, P. Podini for assistance with electron microscopy, G. Dina and A. Cattaneo for technical support and Y. Poitelon for artwork. This study was supported by the Federazione Italiana Sclerosi Multipla (FISM) (grant 2007/PC/01) and the Compagnia di San Paolo (C.T.); by the US National Institute of Health (grants R01-NS045630 (M.L.F.), R01-NS055256 (L.W.), R01-GM64750 (C.P.B.) and RO1-NS26001 (J.L.S.)); by Telethon Italia (grants GGP08021 (M.L.F.), GGP071100 (L.W.) and GPP10007 (C.T., L.W. and M.L.F.)). C.T. is a recipient of a FISM Transition Career Award.

AUTHOR CONTRIBUTIONS

R.L.M. conducted most of the experiments. F.C. and A.Q. performed morphological and ultrastructural analyses of sciatic nerves and ventral roots. K.H., C.P.B., M.L.F. and L.W. provided transgenic lines and helped with discussions. A.B. performed the mass spectrometry analyses. J.L.S. provided support and initially contributed to the experimental design. C.T. designed the experimental plan, supervised the project and wrote the paper. All authors commented on the paper.

COMPETING FINANCIAL INTERESTS

The authors declare no competing financial interests.

Published online at http://www.nature.com/natureneuroscience/.
Reprints and permissions information is available online at http://www.nature.com/reprints/index.html.

1. Taveggia, C. *et al.* Neuregulin-1 type III determines the ensheathment fate of axons. *Neuron* **47**, 681–694 (2005).
2. Michailov, G.V. *et al.* Axonal neuregulin-1 regulates myelin sheath thickness. *Science* **304**, 700–703 (2004).
3. Willem, M. *et al.* Control of peripheral nerve myelination by the β-secretase BACE1. *Science* **314**, 664–666 (2006).
4. Hu, X. *et al.* Genetic deletion of BACE1 in mice affects remyelination of sciatic nerves. *FASEB J.* **22**, 2970–2980 (2008).
5. Hu, X. *et al.* Bace1 modulates myelination in the central and peripheral nervous system. *Nat. Neurosci.* **9**, 1520–1525 (2006).
6. Yang, P., Baker, K.A. & Hagg, T. The ADAMs family: coordinators of nervous system development, plasticity and repair. *Prog. Neurobiol.* **79**, 73–94 (2006).
7. Shirakabe, K., Wakatsuki, S., Kurisaki, T. & Fujisawa-Sehara, A. Roles of Meltrin β/ADAM19 in the processing of neuregulin. *J. Biol. Chem.* **276**, 9352–9358 (2001).
8. Yokozeki, T. *et al.* Meltrin beta (ADAM19) mediates ectodomain shedding of Neuregulin beta1 in the Golgi apparatus: fluorescence correlation spectroscopic observation of the dynamics of ectodomain shedding in living cells. *Genes Cells* **12**, 329–343 (2007).
9. Wakatsuki, S., Yumoto, N., Komatsu, K., Araki, T. & Sehara-Fujisawa, A. Roles of meltrin-β/ADAM19 in progression of Schwann cell differentiation and myelination during sciatic nerve regeneration. *J. Biol. Chem.* **284**, 2957–2966 (2009).
10. Sagane, K. *et al.* Ataxia and peripheral nerve hypomyelination in ADAM22-deficient mice. *BMC Neurosci.* **6**, 33 (2005).
11. Ozkaynak, E. *et al.* Adam22 is a major neuronal receptor for Lgi4-mediated Schwann cell signaling. *J. Neurosci.* **30**, 3857–3864 (2010).
12. Freese, C., Garratt, A.N., Fahrenholz, F. & Endres, K. The effects of alpha-secretase ADAM10 on the proteolysis of neuregulin-1. *FEBS J.* **276**, 1568–1580 (2009).
13. Horiuchi, K., Zhou, H.M., Kelly, K., Manova, K. & Blobel, C.P. Evaluation of the contributions of ADAMs 9, 12, 15, 17, and 19 to heart development and ectodomain shedding of neuregulins β1 and β2. *Dev. Biol.* **283**, 459–471 (2005).
14. Blobel, C.P. ADAMs: key components in EGFR signalling and development. *Nat. Rev. Mol. Cell Biol.* **6**, 32–43 (2005).
15. Peschon, J.J. *et al.* An essential role for ectodomain shedding in mammalian development. *Science* **282**, 1281–1284 (1998).
16. Cosgaya, J.M., Chan, J.R. & Shooter, E.M. The neurotrophin receptor p75^{NTR} as a positive modulator of myelination. *Science* **298**, 1245–1248 (2002).
17. Woodhoo, A. *et al.* Notch controls embryonic Schwann cell differentiation, postnatal myelination and adult plasticity. *Nat. Neurosci.* **12**, 839–847 (2009).
18. Zampieri, N., Xu, C.F., Neubert, T.A. & Chao, M.V. Cleavage of p75 neurotrophin receptor by α-secretase and γ-secretase requires specific receptor domains. *J. Biol. Chem.* **280**, 14563–14571 (2005).
19. van Tetering, G. *et al.* Metalloprotease ADAM10 is required for Notch1 site 2 cleavage. *J. Biol. Chem.* **284**, 31018–31027 (2009).
20. Weber, S. *et al.* The disintegrin/metalloproteinase Adam10 is essential for epidermal integrity and Notch-mediated signaling. *Development* **138**, 495–505 (2011).
21. Horiuchi, K. *et al.* Cutting edge: TNF-α-converting enzyme (TACE/ADAM17) inactivation in mouse myeloid cells prevents lethality from endotoxin shock. *J. Immunol.* **179**, 2686–2689 (2007).
22. Yang, X. *et al.* Patterning of muscle acetylcholine receptor gene expression in the absence of motor innervation. *Neuron* **30**, 399–410 (2001).
23. Donald, D. A relation between axone diameter and myelination determined by measurement of myelinated spinal root fibers. *J. Comp. Neurol.* **60**, 437–471 (1934).
24. Windebank, A.J., Wood, P., Bunge, R.P. & Dyck, P.J. Myelination determines the caliber of dorsal root ganglion neurons in culture. *J. Neurosci.* **5**, 1563–1569 (1985).
25. Maurel, P. & Salzer, J.L. Axonal regulation of Schwann cell proliferation and survival and the initial events of myelination requires PI 3-kinase activity. *J. Neurosci.* **20**, 4635–4645 (2000).
26. Ogata, T. *et al.* Opposing extracellular signal-regulated kinase and Akt pathways control Schwann cell myelination. *J. Neurosci.* **24**, 6724–6732 (2004).
27. Schwenk, F., Baron, U. & Rajewsky, K. A *cre*-transgenic mouse strain for the ubiquitous deletion of *loxP*-flanked gene segments including deletion in germ cells. *Nucleic Acids Res.* **23**, 5080–5081 (1995).
28. Feltri, M.L. *et al.* Conditional disruption of β1 integrin in Schwann cells impedes interactions with axons. *J. Cell Biol.* **156**, 199–209 (2002).
29. Meyer, D. *et al.* Isoform-specific expression and function of neuregulin. *Development* **124**, 3575–3586 (1997).
30. Ohno, M. *et al.* Nardilysin regulates axonal maturation and myelination in the central and peripheral nervous system. *Nat. Neurosci.* **12**, 1506–1513 (2009).
31. Caescu, C.I., Jeschke, G.R. & Turk, B.E. Active-site determinants of substrate recognition by the metalloproteinases TACE and ADAM10. *Biochem. J.* **424**, 79–88 (2009).
32. Yang, H.C. *et al.* Biochemical and kinetic characterization of BACE1: investigation into the putative species-specificity for β- and β′-cleavage sites by human and murine BACE1. *J. Neurochem.* **91**, 1249–1259 (2004).
33. Thinakaran, G. & Koo, E.H. Amyloid precursor protein trafficking, processing, and function. *J. Biol. Chem.* **283**, 29615–29619 (2008).
34. Schlöndorff, J., Becherer, J.D. & Blobel, C.P. Intracellular maturation and localization of the tumour necrosis factor α convertase (TACE). *Biochem. J.* **347**, 131–138 (2000).
35. Doedens, J.R. & Black, R.A. Stimulation-induced down-regulation of tumor necrosis factor-α converting enzyme. *J. Biol. Chem.* **275**, 14598–14607 (2000).
36. Tellier, E. *et al.* The shedding activity of ADAM17 is sequestered in lipid rafts. *Exp. Cell Res.* **312**, 3969–3980 (2006).
37. Frenzel, K.E. & Falls, D.L. Neuregulin-1 proteins in rat brain and transfected cells are localized to lipid rafts. *J. Neurochem.* **77**, 1–12 (2001).
38. Koo, E.H. & Squazzo, S.L. Evidence that production and release of amyloid β-protein involves the endocytic pathway. *J. Biol. Chem.* **269**, 17386–17389 (1994).
39. Burgess, T.L., Ross, S.L., Qian, Y.X., Brankow, D. & Hu, S. Biosynthetic processing of neu differentiation factor. Glycosylation trafficking, and regulated cleavage from the cell surface. *J. Biol. Chem.* **270**, 19188–19196 (1995).
40. Haass, C., Koo, E.H., Mellon, A., Hung, A.Y. & Selkoe, D.J. Targeting of cell-surface β-amyloid precursor protein to lysosomes: alternative processing into amyloid-bearing fragments. *Nature* **357**, 500–503 (1992).
41. Bozkulak, E.C. & Weinmaster, G. Selective use of ADAM10 and ADAM17 in activation of Notch1 signaling. *Mol. Cell. Biol.* **29**, 5679–5695 (2009).
42. Buser, A.M. *et al.* The myelin protein MAL affects peripheral nerve myelination: a new player influencing p75 neurotrophin receptor expression. *Eur. J. Neurosci.* **29**, 2276–2290 (2009).
43. Tomita, K. *et al.* The neurotrophin receptor p75^{NTR} in Schwann cells is implicated in remyelination and motor recovery after peripheral nerve injury. *Glia* **55**, 1199–1208 (2007).
44. Fricker, F.R. *et al.* Sensory axon-derived neuregulin-1 is required for axoglial signaling and normal sensory function but not for long-term axon maintenance. *J. Neurosci.* **29**, 7667–7678 (2009).
45. Fricker, F.R. *et al.* Axonally derived neuregulin-1 is required for remyelination and regeneration after nerve injury in adulthood. *J. Neurosci.* **31**, 3225–3233 (2011).
46. Moss, M.L., Sklair-Tavron, L. & Nudelman, R. Drug insight: tumor necrosis factor-converting enzyme as a pharmaceutical target for rheumatoid arthritis. *Nat. Clin. Pract. Rheumatol.* **4**, 300–309 (2008).

ONLINE METHODS

Mice and genotyping. Generation of *Tace*-floxed mice has been previously reported[21]. Mice were genotyped by PCR using the following primers: 5′-TTA CTCTTCTTACTAACAGTCCCCTG-3′ and 5′-AACTATCTCAAACAATAAG CTGAAGTG-3′. Homozygous *Tace*-floxed mice were crossed with the *HB9-cre* transgenic line to specifically delete *Tace* in motor neurons, with the *mP0TOT-cre* (*Mpz-cre*) transgenic line to ablate *Tace* in Schwann cells and with the *CMV-cre* transgenic line to generate complete $Tace^{+/-}$ mice. Generation of the *HB9-cre*, *Mpz-cre* and *CMV-cre* transgenic lines has been previously described[22,27,28]. The genotyping was performed by PCR analysis on genomic DNA. PCR was carried out at 94 °C for 30 s, 60 °C for 30 s and 72 °C for 30 s, followed by a 5 min extension at 72 °C for 40 cycles. The expected 850-nucleotide (nt) product for the wild-type allele and 1,000-nt product for the floxed allele were separated on a 1% agarose gel. The presence of the null allele was also determined by PCR on genomic DNA using the following primers: 5′-TTACTCTTCTTAC TAACAGTCCCCTG-3′ and 5′-GGGAGAGCCACACCTTGACC-3′. PCR was carried out at 94 °C for 30 s, 60 °C for 30 s and 72 °C for 30 s, followed by a 5-min extension at 72 °C for 40 cycles. The amplified fragment of 400 nt, corresponding to the null allele, was analyzed on a 1% agarose gel. Generation and analysis of *Nrg1 type* $III^{-/-}$ and *Nrg1 type* $III^{+/-}$ mice have been previously described[1]. All experiments involving animals followed protocols approved by the Animal Care and Use Committee of San Raffaele Scientific Institute.

Cell cultures. Mouse DRG neurons were isolated from embryonic day 14.5 embryos and established on collagen-coated glass coverslips as described[1]. Explants were cycled with fluoroxidine (FUDR, Sigma-Aldrich) to eliminate all non-neuronal cells. Neuronal medium was supplemented with 50 ng ml^{-1} NGF (Harlan, Bioproducts for Science). Primary rat Schwann cells were prepared as described[1] and maintained in DMEM (BioWhittaker), 10% FBS (Invitrogen) and 2 mM L-glutamine (Invitrogen) until used. Rat Schwann cells were added (200,000 cells per coverslip) to establish explant cultures of DRG neurons, and myelination was initiated by supplementing the medium with 50 µg ml^{-1} ascorbic acid (Sigma-Aldrich).

Fc fusion proteins and binding experiments. Established explants of $Tace^{-/-}$, wild-type, and DRG neurons previously infected with shRNA against *Tace* were incubated with supernatant containing ERBB2-ERBB3–Fc and an antibody to human Fc (Jackson ImmunoResearch) as described[1]. Quantification was performed on confocal images from three different experiments (five coverslips per experiment). All images with the same magnification, *z*-stack and laser intensity were analyzed using Image J version 1.44 (US National Institutes of Health).

Lentivirus production and infection. Individual shRNAs clones (TRCN0000031949, TRCN0000031952 and TRCN0000031953) specifically targeting mouse *Tace* were obtained through the RNAi Consortium (Open Biosystems). Lentiviral vectors were transfected into 293FT cells (Invitrogen) together with packaging plasmids pLP1, pLP2 and pLP/VSVG (Invitrogen) using Lipofectamine 2000 (Invitrogen) according to the manufacturer's instructions. As a control, we used a vector encoding an shRNA directed against an oligonucleotide (5′-TCGTACGCGCAATACTTCGA-3′) whose sequence had been verified to be nonspecific by a database search against the human and the mouse genomes. The scrambled shRNA–encoding lentiviral vector was cloned in pLL3.7 and produced as described[47]. Lentivirus encoding full length NRG1 type III was generated as described[1]. The cDNA encoding NRG1 type III from the N terminus until the histidine between the identified TACE cleavage sites was amplified by PCR with the following primers: 5′ CAGATCACTAGTATGGAGATTTATTCC CCAGAC 3′ and 5′CACTTTCTCGAGTTAATGTTTGTAGAAGCTGGC 3′; the template used was full length NRG1 type III that was hemagglutinin-tagged in the extracellular region, cloned in a pLenti6/V5 plasmid with standard molecular biology techniques and confirmed by sequencing.

Viral supernatants were collected 48 h after transfection, centrifuged at 1,500 *g* for 15 min, divided into aliquots for one-time use and frozen at −80 °C. Freshly plated Schwann cells (10^6 cells per 100-mm plate) were incubated for 2 d with viruses at a 2/3 dilution (vol/vol) in DMEM, 10% FBS and 2 mM L-glutamine supplemented with forskolin and recombinant human NRG1 (EGF domain, R&D Systems). Cells were expanded for 1 week more and maintained for 3 d in Schwann cell medium before use. Protein knockdowns were confirmed by western blotting. Mouse DRG neuronal explants were infected the day after the dissection and left in the presence of the virus for 24 h, after which cultures were either purified of endogenous Schwann cells to obtain pure DRG neurons by cycling them with antimitotic reagents, or cultured with endogenous Schwann cells. In the latter case, both DRG neurons and mouse primary Schwann cells were infected.

Electron microscopy and morphological analyses. Semithin and ultrathin sections were obtained as previously described[48]. Tissues were removed and fixed with 2% (vol/vol) glutaraldehyde in 0.12 M phosphate buffer, postfixed with 1% (wt/vol) osmium tetroxide and embedded in Epon (Fluka). Semithin sections (0.5 to 1 µm thick) were stained with toluidine blue and examined by light microscopy (Olympus BX51). Ultrathin sections (100 to 120 nm thick) were stained with uranyl acetate and lead citrate and examined by electron microscopy (Leo 912 Omega). Digitized nonoverlapping semithin sections images from corresponding levels of the sciatic nerve were obtained with a digital camera (Leica DFC300F) using a ×100 objective. *g* ratio measurements were performed on digitized nonoverlapping electron micrographs images. *g* ratios were determined by dividing the mean diameter of an axon without myelin by the mean diameter of the same axon with myelin.

To determine the size distribution of myelinated fibers in sciatic nerves, diameters of all fibers in at least ten images of randomly chosen representative images were measured and binned based on their width. All measurements were acquired on ×100 semithin section images using the ImageJ software (US National Institutes of Health).

TACE and BACE1 cleavage reaction. Human recombinant TACE (1 µg; R&D Systems cat. no. 930-ADB) was incubated with 2 µg of human recombinant NRG1 β1 (R&D Systems cat. no. 396-HB, residues 176–246), which differs from the mouse sequence by one amino acid upstream of the EGF domain, for 16 h at 37 °C in the presence of $ZnCl_2$ and then separated on a Tris-tricine gel together with native, uncleaved NRG1 β1 protein for comparison. The gel was stained with Coomassie blue and then processed for mass spectrometry analysis.

To test TACE and BACE1 cleavage effects of NRG1 signaling, 1 or 2 µg of human recombinant TACE or BACE1 (R&D Systems cat. no. 931-AS) were incubated with 0.5 µg of human recombinant NRG1 β1 for 16 h at 37 °C. Cleaved NRG1 β1 was used to stimulate serum-starved rat primary Schwann cells for 20 min at 37 °C. Cells were then lysed and analyzed by western blot for PI3K-intermediate pathways.

MALDI-TOF MS analyses. Bands of interest were excised from gels, subjected to reduction by 10 mM dithiothreitol and alkylation by 55 mM iodoacetamide, and finally digested overnight with endoproteinase Glu-C (Roche). Supernatant mixture from the digestion (10 µl) was acidified with formic acid up to a final concentration of 10% (vol/vol), desalted with Stage Tip µC18 (Stage Tip packed with uC18 reverse phase resin Proxeon Biosystem)[49] and analyzed on a MALDI-TOF Voyager-DE STR (Applied Biosystems) mass spectrometer using the dried droplet technique and α-cyano-4-hydroxycinnamic acid as matrix. Spectra were acquired in the reflector positive-ion mode, accumulated over a mass range of 750–4,000 Da with a mean resolution of about 15,000, then internally calibrated using matrix signals and Glu-C autolysis peaks and processed using Data Explorer software version 4.0.0.0 (Applied Biosystems). Assignment of singly protonated species peaks was carried out manually using GPMAW software (version 8.10).

RNA isolation and measurements. Total RNA was isolated from purified rat Schwann cells, purified mouse DRG neurons and mouse spinal cord using Trizol (Roche), according to the manufacturer's instructions. Total RNA was reverse-transcribed to cDNA as previously described[50]. Aliquots of the reverse transcription products were tested in parallel using a primer pair for *Tace* (5′-TTGAAGAATACTTGTAAATT-3′ and 5′-GGGTTGTAATAAGCTTTT GG-3′; 94 °C for 30 s, 52 °C for 30 s and 72 °C for 60 s, followed by a 5 min extension at 72 °C for 30 cycles).

Preparation of detergent lysates and immunoblotting. Tissues and cell cultures were Dounce-homogenized in a lysis buffer containing 2% (wt/vol) SDS, 95 mM NaCl, 10 mM EDTA, phosphatase inhibitor (PhoSTOP, Roche) and protease inhibitors (Complete-Mini EDTA free, Roche). Homogenates were boiled

doi:10.1038/nn.2849

for 5 min and centrifuged for 10 min at 16,800*g* at 16 °C. Supernatants were divided into aliquots and stored at −80 °C until used. Protein concentrations were determined by the bicinchoninic acid method (Pierce); samples (20–40 µg of protein) were fractionated by SDS-PAGE and blotted onto nitrocellulose (Protran Biosciences). Membranes were blocked in 5% BSA, 0.05% sodium azide in TBST (0.1% Triton X-100 in TBS). Appropriate regions were excised, incubated with specific primary and secondary antibodies, washed in TBST and developed with the SuperSignal chemiluminescent substrate (Pierce). For quantitative western blotting, filters were analyzed using the Odyssey Infrared Imaging System (LI-COR Biosciences) according to the manufacturer's instructions.

Antibodies and immunofluorescence. Mouse monoclonal antibodies included antibodies to MBP (SMI-94, SMI-99) and neurofilament (SMI-31 and SMI-32) (Sternberger Monoclonals) and to Notch-1 (NICD) (Chemicon). Rabbit polyclonal antibodies included antibodies to NRG1 (sc-348) (Santa Cruz); MAG[1]; MPZ (M. Filbin); actin (Sigma-Aldrich); peripherin, TACE and $p75^{NTR}$ (Chemicon); and Ser473 p-AKT and total AKT (Cell Signaling). Chicken antibodies were to neurofilament M (Covance). Secondary antibodies conjugated to rhodamine, fluorescein, coumarin, Cy5, or horseradish peroxidase were obtained from Jackson ImmunoResearch. Infrared secondary antibodies for quantitative western blotting (goat anti-rabbit and goat anti-mouse IRDye 680 or IRDye 800) were obtained from LI-COR Biosciences. Cocultures were fixed in 4% (wt/vol) paraformaldehyde, permeabilized in 100% methanol at −20 °C for 15 min, stained as described[1] and examined by epifluorescence on a Nikon E800 microscope and by confocal microscopy on a Zeiss LSM 510 or on a Leica SP5.

Statistical analyses. Statistical analyses (Fisher's exact test, the chi-squared test and Student's *t*-test) were performed using the Prism Software package (GraphPad). $P < 0.05$ was taken as the limit of statistical significance.

47. Maurel, P. *et al.* Nectin-like proteins mediate axon Schwann cell interactions along the internode and are essential for myelination. *J. Cell Biol.* **178**, 861–874 (2007).
48. Quattrini, A. *et al.* β4 integrin and other Schwann cell markers in axonal neuropathy. *Glia* **17**, 294–306 (1996).
49. Shevchenko, A., Wilm, M., Vorm, O. & Mann, M. Mass spectrometric sequencing of proteins silver-stained polyacrylamide gels. *Anal. Chem.* **68**, 850–858 (1996).
50. Wrabetz, L. *et al.* A minimal human MBP promoter-*lacZ* transgene is appropriately regulated in developing brain and after optic enucleation, but not in shiverer mutant mice. *J. Neurobiol.* **34**, 10–26 (1998).